Heliyon 10 (2024) e29814

Contents lists available at ScienceDirect

Heliyon

journal homepage: www.cell.com/heliyon

Research article

Nanoplastics inhibit carbon fixation in algae: The effect of aging

Ziyi Sun [a], Shuang Zhang [a], Tianying Zheng [a], Caijiao He [a], Jiang Xu [a], Daohui Lin [a,**], Luqing Zhang [b,*]

[a] Zhejiang Provincial Key Laboratory of Organic Pollution Process and Control, Department of Environmental Science, Zhejiang University, Hangzhou, 310058, China

[b] Institute of Pesticide and Environmental Toxicology, The Key Laboratory of Molecular Biology of Crop Pathogens and Insects, College of Agricultural and Biotechnology, Zhejiang University, Hangzhou, 310058, China

ARTICLE INFO

Keywords:
Photosynthetic toxicity
Recovery
UV aging
Hetero-agglomeration
Molecular responses

ABSTRACT

Despite the considerable efforts devoted to the toxicological assessment of nanoplastics, the effect of UV-irradiation induced aging, a realistic environmental process, on the toxicity of nanoplastics toward microalgae and its underlying mechanisms remain largely unknown. Herein, this study comparatively investigated the toxicities of polystyrene nanoplastics (nano-PS) and the UV-aged nano-PS on the eukaryotic alga *Chlorella vulgaris*, focusing on evaluating their inhibitory effects on carbon fixation. Exposure to environmentally relevant concentrations (0.1–10 mg/L) of nano-PS caused severe damage to chloroplast, inhibited the photosynthetic efficiency and electron transport, and suppressed the activities of carbon fixation related enzymes. Multi-omics results revealed that nano-PS interfered with energy supply by disrupting light reactions and TCA cycle and hindered the Calvin cycle, thereby inhibiting the photosynthetic carbon fixation of algae. The above alterations partially recovered after a recovery period. The aged nano-PS were less toxic than the pristine ones as evidenced by the mitigated inhibitory effect on algal growth and carbon fixation. The aging process introduced oxygen-containing functional groups on the surface of nano-PS, increased the hydrophilicity of nano-PS, limited their attachment on algal cells, and thus reduced the toxicity. The findings of this work highlight the potential threat of nanoplastics to the global carbon cycle.

1. Introduction

Due to the surge in plastic wastes and the unintentional release from plastic containing products, microplastics (<5 mm in diameter) are widespread in the aquatic environment with their environmental concentration increasing rapidly, posing a potential threat to aquatic ecosystems [1,2]. Numerous studies have shown that microplastics are toxic to various aquatic organisms, including fish, algae, and invertebrates [3]. Comparatively, research on nanoplastics, which are smaller (<100 nm), is still in its infancy [4]. Studies suggested that nanoplastics might be more toxic with a mode of action different from microplastics. For example, nanoplastics induced greater retardation in the reproduction and population growth of *Brachionus plicatilis* than microplastics due to selective generation of oxidative stress and enhanced metabolic deficiency [5]. It was estimated that nanoplastics might be present in the environment at a concentration up to 17 orders of magnitude higher than microplastics [6], highlighting the urgency of an in-depth

* Corresponding author.
** Corresponding author.
E-mail addresses: lindaohui@zju.edu.cn (D. Lin), zhangluqing@zju.edu.cn (L. Zhang).

https://doi.org/10.1016/j.heliyon.2024.e29814
Received 5 April 2024; Received in revised form 14 April 2024; Accepted 15 April 2024
Available online 16 April 2024

understanding of their impact on the ecological environment. However, current studies regarding the aquatic toxicity of nanoplastics mainly focused on the marine environment with less attention paid to the freshwater environment which is more susceptible to frequent human activities.

Microalgae, as the primary producers in aquatic ecosystems, have fixed approximately half of the atmospheric carbon dioxide and one-third of anthropogenic carbon over the past century [2,7]. They facilitate growth through photosynthesis and convert atmospheric CO_2, a significant carbon source, into glucose [8]. Each year, approximately 100 billion tons of CO_2 are naturally sequestered, with microalgae contributing around 33 billion tons to this process [9]. Mounting evidence shows that micro/nanoplastics could induce oxidative stress and physical damage to microalgae, leading to inhibited photosynthesis and ultimately a reduction in biomass [10,11]. Theoretically, photosynthetic reactions consist of light reactions which capture and store light energy and carbon reactions wherein the captured carbon dioxide is completely fixed through the Calvin cycle [12]. A number of studies have observed that micro/-nanoplastics induced disturbances in the light reactions as indicated by altered chlorophyll levels and chlorophyll fluorescence parameters [10,11]. The inhibition of nanoplastics on the light reactions of algae which provide ATP and NADPH for the carbon reaction is likely to impair the photosynthetic carbon fixation, a process that is often overlooked. Recently, it is reported that polystyrene nanoplastics interfered with the photosynthetic carbon fixation of a cyanobacterium *Synechocystis* sp. in a manner different from microplastics [13]. Eukaryotic microalgae constitute one of the most diverse groups of photosynthetic autotrophs on earth. Unlike prokaryotic algae, eukaryotic algae possess chloroplasts and use non-photochemical quenching (NPQ) for photoprotection, exhibiting higher photosynthetic efficiency. Accordingly, the findings obtained from the prokaryotic algae may not be fully applicable to the eukaryotic species since they are completely different from each other in structure and function. To date, the effect of nanoplastics on the carbon fixation of eukaryotic microalgae and its underlying molecular mechanism are still unknown. Moreover, nanoparticle exposure may exert a lasting but recoverable inhibitory effect in addition to instant toxicity [14]. It is therefore essential to integrate the recovery results for a comprehensive understanding of the nanoplastic toxicity toward algae.

When being discharged into the aquatic environments, micro/nanoplastics would undergo ultraviolet irradiation, leading to some degree of aging [15]. Light-induced aging may alter the physicochemical properties of micro/nanoplastics (e.g. particle size, surface functionality, etc.), influencing their interactions with biota. Studies have shown that aged micro/plastics exhibited different toxic effects compared with their pristine counterparts. For example, UV aged polyvinyl chloride microplastics (mPVC) induced more severe intestinal damage in zebrafish than pristine mPVC [16,17]. UV aging exacerbated the neurotoxicity of polystyrene microplastics to *Caenorhabditis elegans*, but mitigated their inhibitory effect on the reproduction of *Daphnia magna* [18]. A previous study reported that pristine polystyrene nanoplastics (nano-PS) induced greater CO_2 assimilation and microcystin synthesis in a cyanobacterium *Microcystis aeruginosa* than aged PS microplastics, indicating that UV-aging did not necessarily increase the toxicity [19]. Despite the available toxicity data of the aged micro/nanoplastics, the influence of light-induced aging on the toxicity of nanoplastics to eukaryotic microalgae remains unclear.

The present study was therefore aimed to investigate the effect of nanoplastics on carbon fixation of algae as influenced by aging. Nano-PS, which is known to be prevalent in freshwater environments, was selected. *Chlorella vulgaris*, a unicellular eukaryotic microalga, was used as a model organism. The inhibitory effect of pristine and aged nano-PS on the growth and carbon fixation related processes of *C. vulgaris* as well as the recovery of the inhibitory effects were specifically studied. Multi-omics were employed to analyze molecular responses of the algae to nano-PS exposure. The findings of this work will contribute to toxicological assessment of nanoplastics.

2. Materials and methods

2.1. Preparation and characterization of nano-PS

Nano-PS suspension was purchased from Baseline, Inc. (China), with the initial particle size of 100 nm. The nano-PS suspension was subjected to dialysis (molecular weight cut off 14000 D) against deionized water for 4 h to obtain the stock solution of pristine nano-PS (1000 mg/L). Aged nano-PS was obtained by irradiating the pristine nano-PS stock solution with a 500 W mercury lamp for 96 h in a photochemical reactor (XPA-7, XUJIANG, China). The morphology, structure, and physicochemical properties of the nano-PS were characterized by scanning electron microscopy (SEM, SIRION-100, FEI, USA), transmission electron microscopy (TEM, Hitachi H-7650, Japan), Fourier transform infrared spectroscopy (FTIR, Nicolet 6700, Thermo Fisher Scientific, USA), X-ray photoelectron spectroscopy (XPS, Escalab 250Xi, Thermo Fisher Scientific, USA), contact angle tester (WCA, OSA200-T, NBSI, China), and zeta sizer (Nano ZS90, Malvern, UK).

2.2. Exposure and recovery experiments

C. vulgaris was obtained from the Institute of Wuhan Hydrobiology, Chinese Academy of Sciences, and was cultured in BG11 medium with components listed in Table S1 in the Supporting information (SI). The algae were cultivated in a light incubator (light: dark of 14: 10 h) at 22 ± 1 °C and 60 % humidity. In the exposure experiment, exponentially growing algae (1×10^5 cells mL^{-1}) were cultured in 250 mL Erlenmeyer flasks and maintained in an incubator shaker (120 rpm) under illumination of 100 μE m^{-2} s^{-1} (light/dark of 14/10 h) at 22 ± 1 °C. Pristine or aged nano-PS stock solutions were then added to achieve the final concentrations of 0–64 mg/L. In the recovery experiment, the algal cells after the 96-h exposure to nano-PS were collected by centrifugation (5000*g*, 10 min) and washed three times with fresh BG11 medium. The resulting algal pellets were subsequently diluted with BG11 medium to a density of 1×10^5 cells mL^{-1} and cultured for 96 h. At the end of both exposure and recovery periods, densities of algal cells were determined

using a hemocytometer and the median effect concentration (EC_{50}) was calculated using the logistic model [20]. In addition, the ribulose-1,5-bisphosphate carboxylase/oxygenase (RuBisCo) activity, adenosine triphosphate synthase (FoF1-ATPase) activity, glucose hexaphosphate dehydrogenase (G6PDH) activity, CO_2 fixation rate, organelle integrity, levels of photosynthetic pigments, parameters of chlorophyll fluorescence were analyzed.

2.3. Settling experiments

Nano-PS homo-agglomeration and hetero-agglomeration with algal cells were evaluated following the methods described in our previous work and detailed in SI [21]. The absorbances of individual or mixed nano-PS and algal suspensions were monitored over time. Based on the model fitting, the discrepancy between the optical density (OD) values of co- (mix) and additive- (sum) settling curves were calculated. A higher ΔOD (OD_{mix} - OD_{sum}) value indicates stronger agglomeration.

2.4. Carbon fixation capacity assessment

To evaluate the effect of nano-PS on the carbon fixation capacity of algae, glucose content, activities of carbon fixation-related enzymes, and carbon dioxide fixation rate were determined. After the 96-h exposure or recovery, the algal cells were collected by centrifugation (5000*g*, 10 min, 4 °C) followed by thorough rinse with phosphate-buffered saline (PBS, pH 7.0). The harvested algal cells were resuspended in 0.5 mL PBS (pH 7.0) and then freeze-thawed three times with liquid nitrogen to completely disrupt the cell structure. The activities of RuBisCo, FoF_1-ATPase, and G6PDH as well as the content of glucose were measured using assay kits according to the manufacturer's protocol as detailed in SI.

To determine CO_2 fixation rate, carbon-free Selenite Enrichment (SE) medium was used for algal culture in the exposure and recovery experiments to ensure that CO_2 in the air is the sole source of carbon. The components of the carbon-free SE medium are listed in Table S2. After centrifugation (4000*g*, 10 min, 4 °C) and thorough wash, the algal cells were collected and divided into two subsamples. One subsample was dried, sieved, and analyzed for carbon content using an elemental analyzer (Elementar Vario EL Cube, Germany), and the other one was dried at 105 °C for 16 h and weighed to determine its dry weigh [22]. The elemental compositions of the algae are listed in Table S3. The carbon dioxide fixation rate is calculated by the following formula [23]:

$$\text{Carbon dioxide fixation rate} = P \times C \times \frac{M_{CO_2}}{M_C} \quad (1)$$

where P ($g_{biomass}\ L^{-1}\ d^{-1}$) is the biomass productivity; C (w/w) is the carbon content from elemental analysis; M (g mol^{-1}) is the molar mass.

2.5. Determination of photosynthetic pigments and chlorophyll fluorescence

Changes in photosynthetic pigments can directly reflect the degree of photosynthesis impairment. Concentrations of Chlorophyll *a*, chlorophyll *b*, carotenoids, and phycobiliproteins were determined following the previously described methods with details given in SI [24,25].

Chlorophyll fluorescence parameters including the optimal photochemical efficiency of PSII in the dark (F_v/F_m) and the maximum photosynthetic electron transport rate (ETR_{max}) were analyzed using a dual-channel chlorophyll fluorometer (Dual-PAM-100, Walz, Germany) [26]. The F_v/F_m value was normalized by the values of the blank control group.

2.6. Ultrastructure observations

Transmission electron microscope (TEM) was used to observe the ultrastructural changes induced by the nano-PS. Algal cells collected from exposure and recovery experiments were fixed overnight in 2.5 % glutaraldehyde at 4 °C and stained with 1 % osmium acid for 2 h. Subsequently, the algal samples were subjected to dehydration, embedding, and section. After post-staining with lead citrate and uranyl acetate, the ultrastructure of the algal cells was finally observed on a TEM (Hitachi H-7650, Japan).

2.7. Metabolomic analysis

Algal cells were harvested by centrifugation (4 °C, 5000*g*, 10 min) after exposure to pristine or aged nano-PS (10 mg/L) for 96 h for metabolomic and transcriptomic analyses. Algal cells exposed to nano-PS followed by 96-h recovery were also collected. After repeated freezing and thawing, cell pellets were extracted with 1.2 mL of methanol-water-chloroform (5:2:2, v/v/v) solution via ultrasonic bath (200 W) for 1 h, and 24 μg of ribitol was added as internal standard. The extracted slurry was centrifuged (twice at 12000*g* for 10 min at 4 °C), and 400 μL aliquots of the supernatant were transferred to a 2 mL chromatography vial. After vacuum drying, 50 μL of methoxyamine hydrochloride (20 mg/mL in pyridine) and 80 μL of N-methyl-*n*-(trimethylsilane) trifluoroacetamide (MSTFA) were added to the residues as derivatizing agents. The gas chromatography-mass spectrometry (GC-MS, QP2020NX, SHIMADZU, Japan) was used to analyze the metabolites in algal cells as described in a previous study [27]. The Kyoto Encyclopedia of Genes and Genomes (KEGG, http://www.genome.jp/kegg/) and the Human Metabolome Database (HMDB, http://www.hmdb.ca/) were used for identification of metabolites and analysis of metabolic pathway. Principal component analysis (PCA) and partial least squares-discriminant

analysis (PLS-DA) were conducted using MetaboAnalyst 3.0 to determine the differences in metabolic profiles between control and treated groups. The details for metabolite detection and analysis are provided in SI.

2.8. Transcriptomic analysis

The collected algal cells were immediately frozen using liquid nitrogen. Transcriptome (mRNA) was analyzed as previously described [28]. Briefly, total RNA was isolated using TRIzol reagent (Invitrogen, USA) and the genomic DNA was removed using DNase I (TaKara, Japan). Then the quality of mRNA samples was determined using a bioanalyzer (Agilent 2100, Agilent, USA). After quantification with an ultra-micro spectrophotometer (ND-2000, NanoDrop Technologies, USA), RNA library was prepared using the TruSeq™ RNA Sample Preparation Kit (Illumina, USA) and sequenced on an Illumina Hiseq X ten sequencer (Illumina, USA). Bioinformatics analysis was performed on the biocloud platform of Shanghai Majorbio Bio-pharm Technology Co., Ltd. (https://cloud.majorbio.com/). Differentially expressed genes (DEGs) are required to satisfy the criteria of $|\log_2(\text{fold change})| \geq 1$ and $P < 0.05$. KEGG (http://www.genome.jp/kegg/) was used for gene functional analysis. A KEGG pathway was considered as significant if the *P*-value was ≤ 0.05. The expression of 14 DEGs was validated by real-time polymerase chain reaction (RT-PCR), and the primers are shown in Table S4.

2.9. Statistical analyses

All experiments were conducted at least in triplicate, and the results are expressed as means ± standard deviation. Data analysis

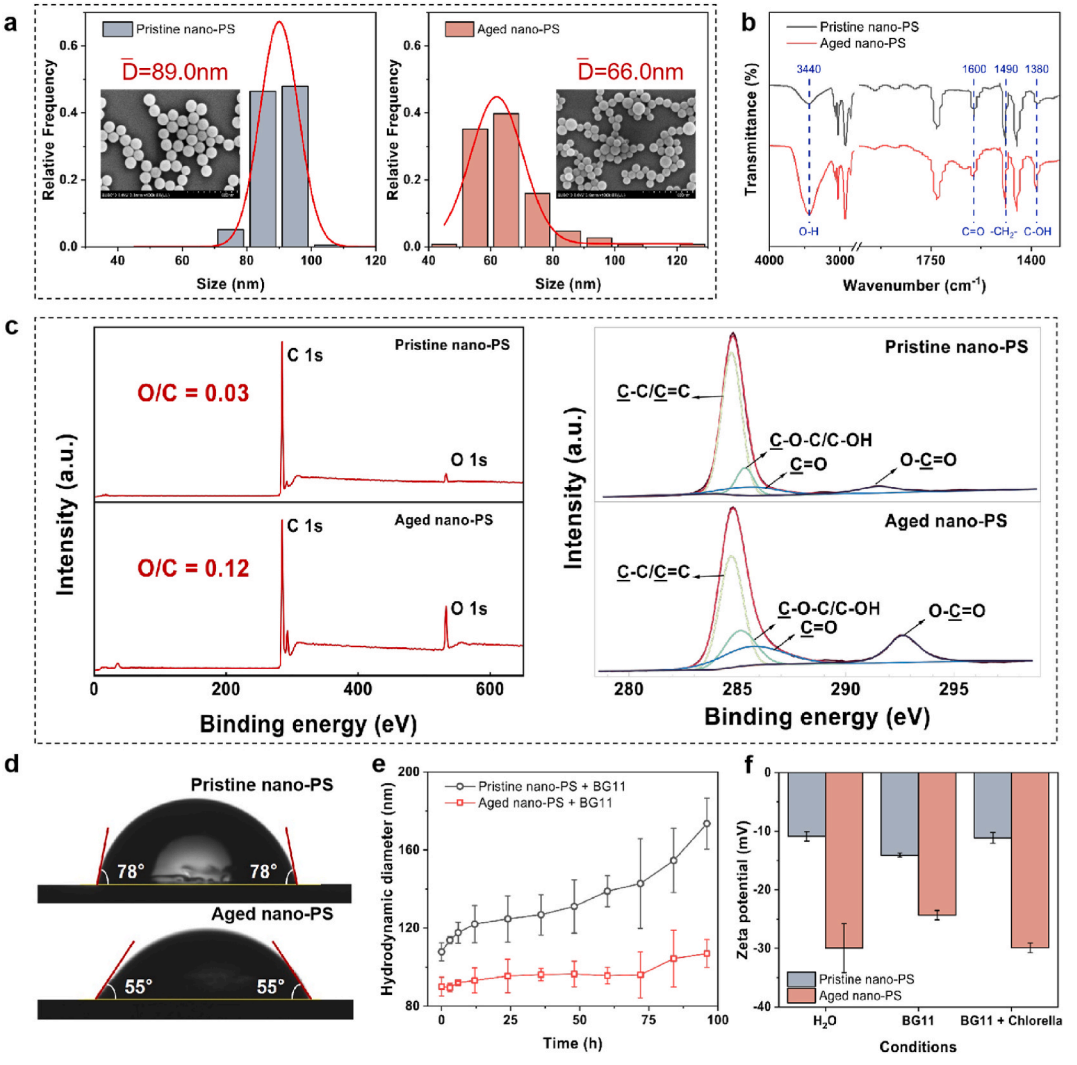

Fig. 1. Characteristics of nano-PS. (a) SEM images and particle size distribution; (b) FTIR spectrum; (c) XPS survey spectra and C1s spectra; (d) contact angles; (e) hydrodynamic diameters and (f) zeta potentials of the nano-PS in the medium.

was performed using SPSS (Statistic 25, IBM, USA). T-test or one-way analysis of variance (ANOVA) followed by Duncan's test was used to determine the significance between treatments. $P < 0.05$ was considered statistically significant.

3. Results and discussion

3.1. Characterization of nano-PS

Typical SEM and TEM images and size distributions of the pristine and aged nano-PS are shown in and S1. The pristine nano-PS had a smooth spherical shape and showed a relatively uniform size distribution with an average size of 89.0 ± 4.0 nm (n = 100). In contrast, the aged nano-PS particles exhibited a broader particle size distribution with an average of 66.0 ± 8.8 nm (n = 100), and the surface of some PS nanospheres became uneven.

Fig. 1b shows the FTIR spectra of the nano-PS. For both nano-PS, the peak observed at 1490 cm^{-1} corresponds to the bending vibration of $–CH_2-$ [29]. The spectra of aged nano-PS exhibited stronger tensile vibration of phenolic hydroxyl groups (C–OH) at 1380 cm^{-1}, tensile vibration of carbonyl groups (C═O) at 1600 cm^{-1}, and stretching vibration of hydroxyl (-OH) at 3440 of cm^{-1} than the pristine nano-PS, suggesting the introduction of oxygen-containing functional groups on the nano-PS surfaces as a result of UV-aging.

The functional groups on the nano-PS surfaces were further analyzed by XPS. As shown in Fig. 1c, the oxygen-to-carbon ratio of the nano-PS increased from 0.03 to 0.12 after aging, indicating an increase in oxygen-containing functional groups during the aging process. C 1s spectra of the nan-PS were fitted to 4 peaks at binding energies of 284.7, 285.3, 285.7, and 291.5 eV, corresponding to carbon atoms in aromatic rings (C–C/C═C), epoxy/hydroxyl (C–*O*–C/C–OH), carbonyl (C═O), and carboxyl (O–C═O) groups, respectively [30]. After the UV aging, the relative content of C–*O*–C/C–OH, C═O, and O–C═O increased markedly from 13 % to 23 %, 12 %–24 %, and 8 %–17 %, respectively. The combination of FTIR and XPS results suggested that the introduced functional groups were likely present as hydroxyl, aldehyde, and ester.

The contact angle is commonly used to describe the surface hydrophobicity of nanoparticles. As evident in Fig. 1d, the aged nano-PS is more hydrophilic with the smaller contact angle (55°) than the pristine nano-PS (78°), which is attributable to an increase in the surface polarity of nano-PS resulted from the introduction of O-containing functional groups [31]. The hydrodynamic diameter size of the pristine nano-PS increased with time and was consistently higher than that of the aged-PS (Fig. 1e). The ionization of oxygen functional groups could enhance the surface electronegativity of nano-PS (Fig. 1f), resulting in increased electrostatic repulsion and improved stability in the medium [31].

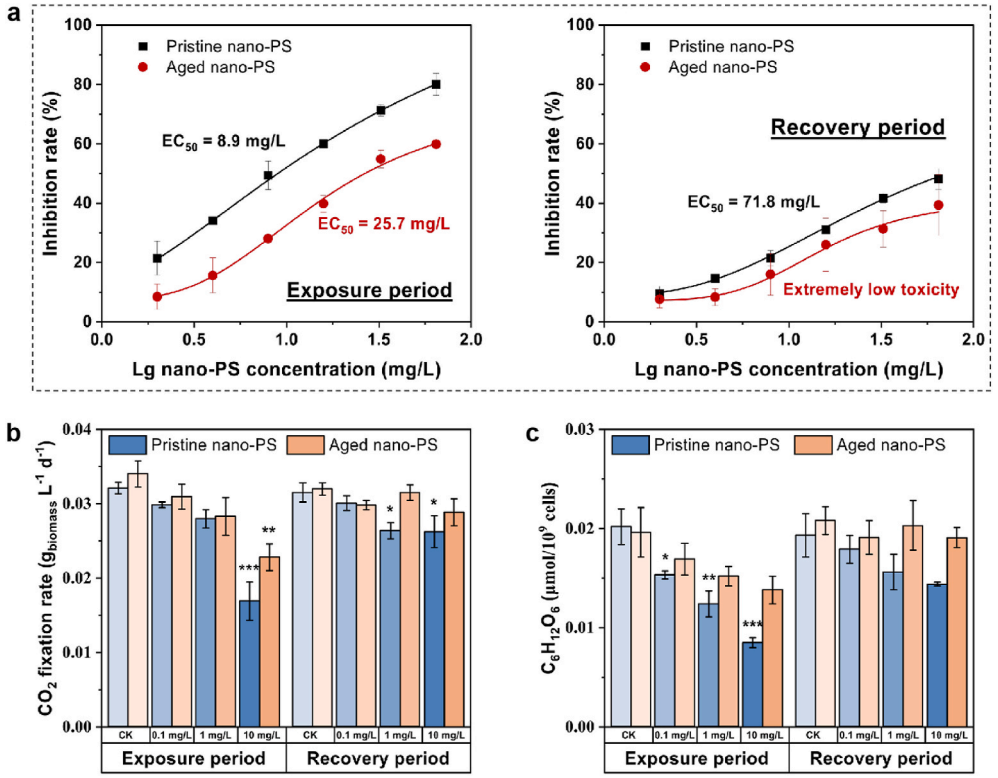

Fig. 2. (a) Dose-response curves of the pristine and aged nano-PS to algae during the exposure and recovery periods. Changes in (b) CO_2 fixation rate and (c) glucose content of algal cells. Error bars represent standard deviations (n = 3). In Panels b and c, * denotes significant differences from the controls, $^*P < 0.05$, $^{**}P < 0.01$, $^{***}P < 0.001$.

3.2. Persistence and recovery of the inhibitory effect on photosynthetic carbon fixation

As shown in Fig. 2a, both pristine and aged nano-PS inhibited algal growth in a dose-dependent manner. The 96-h EC_{50} values of the pristine and aged nano-PS were calculated to be 8.9 and 25.7 mg/L, respectively, indicating the lower toxicity of the aged nano-PS than the pristine nan-PS. A similar result that UV-aging relieved the cytotoxicity of nano-PS was also previously reported [30]. After recovery for 96 h, neither of the two nano-PS reached 50 % inhibition even at the highest test concentration (64 mg/L), although the inhibition rate of the pristine nano-PS was still higher than that of the aged nano-PS. This indicates that the inhibitory effect on algal growth persisted but was alleviated during the recovery period. Such persistent but recoverable toxicity of nano-PS has also been observed in *Eriocheir sinensis* [14].

CO_2 fixation rates of nano-PS-exposed algae in the exposure and recovery stages are displayed in Fig. 2b. During the exposure period, a dose-dependent reduction in the CO_2 fixation rate was observed in both the pristine and aged nano-PS treatments. Notably, the CO_2 fixation rate of the algae exposed to the aged nano-PS at high concentration (10 mg/L) was much higher ($P < 0.05$) as compared to the pristine nano-PS. After the 96-h recovery, the CO_2 fixation rate of the algae treated with high concentration of nano-PS significantly increased ($P < 0.05$), indicating the recovery of CO_2 fixation.

Through the Calvin cycle, carbon dioxide is fixed and ultimately transformed into glucose, which eventually ends up as the major source of energy and nutrient for algal growth [32]. As a primary end product of carbon fixation, the content of glucose can indirectly reflect the efficacy of the overall carbon fixation process. After the exposure to the pristine nano-PS for 96 h, the glucose content of the algae significantly decreased with increasing concentration (Fig. 2c), suggesting impaired carbon fixation in the cells. In the recovery period, the glucose content of the algae in each treatment group was higher than that in the exposure period, showing a sign of recovery. Compared to the pristine nano-PS treatments, much higher glucose contents were detected in the algal cells treated with the aged nano-PS at the exposure stage, which returned to a level comparable to that in the control group in the subsequent recovery period. Results of CO_2 fixation rate and glucose content determination collectively demonstrated that the nano-PS inhibited the photosynthetic carbon fixation of *C. vulgaris* and that the inhibitory effect was mitigated as a result of aging.

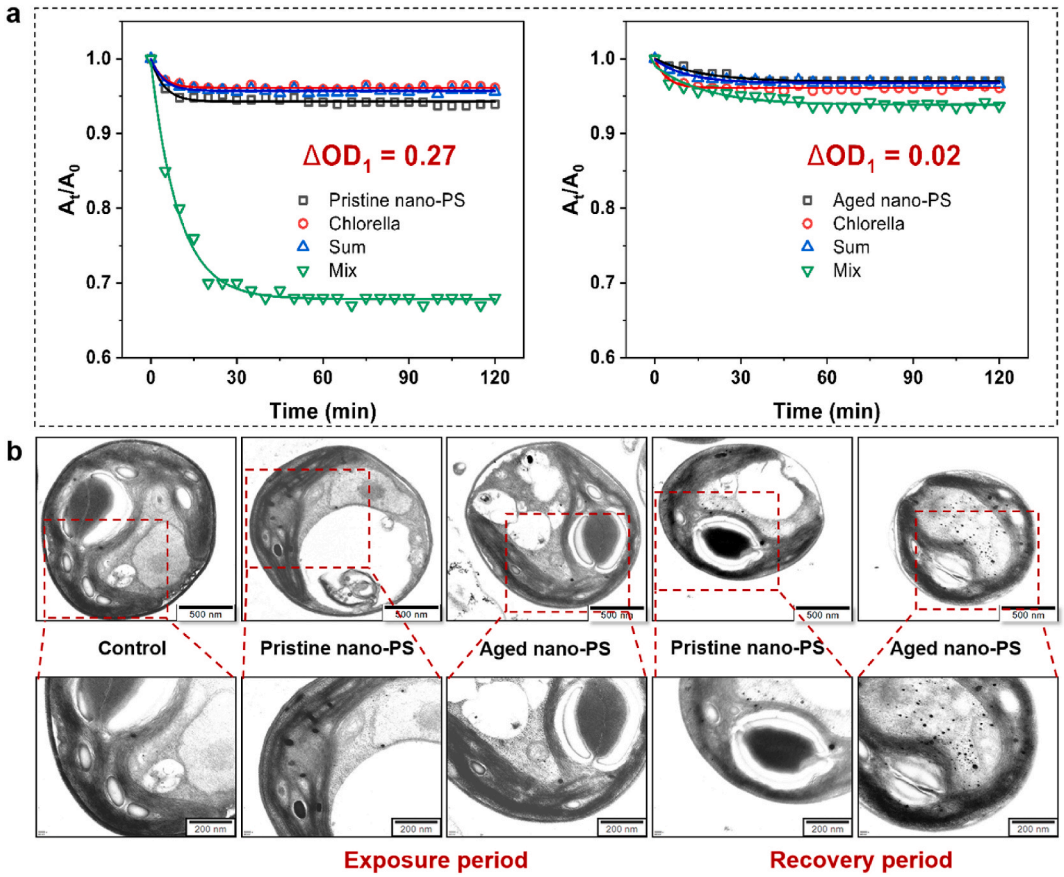

Fig. 3. (a) Settling curves of nano-PS and algae cells. (b) TEM images of the control algae and algae exposed to the nano-PS in the exposure and recovery periods.

3.3. Interactions between nano-PS and algal cells

The individual-, co- (mix), and additive- (sum) settling curves of nano-PS and algal cells are presented in Fig. 3a. Approximately 6 % of pristine nano-PS precipitated during the experimental period, while the settling for the aged nano-PS was 3 %, demonstrating an improvement in dispersion stability by aging. The co-settling curve of the pristine nano-PS and algal cells was much lower than that of the aged nano-PS and algal cells, with ΔOD values calculated to be 0.27 and 0.02 for the pristine and aged nano-PS, respectively (Fig. 3a). The result suggested the much stronger agglomeration of the pristine nano-PS with algae than the aged nano-PS. Synthetic polymers usually have chemically inert hydrophobic surfaces with high affinity to biomolecules such as proteins and lipids, thereby facilitating cell attachment [31,33]. The grafting of oxygen-containing functional groups due to UV-aging reduced the hydrophobicity of nano-PS and increased their electronegativity, resulting in reduced hydrophobic interactions and enhanced electrostatic repulsion between the cell surface and the nano-PS and thereby weaker cell contact. The attachment of nano-PS on cell surfaces might block algal pores or gas exchange, cause shading and mechanical damage to the cell, and trigger ROS generation [11,34]. These reactions might subsequently disrupt the physiological function of various organelles including chloroplasts, thus impairing the photosynthesis and growth of algae [35]. Accordingly, the mitigated toxicity of nanoplastics by aging could be explained by the reduced cell contact.

As shown in Fig. 3b, the untreated algal cells exhibited good structural integrity with thylakoids compactly and orderly arranged in chloroplasts. Following exposure to the pristine nano-PS, cell shrinkage, cytoplasmic vacuolation, and plasmolysis were observed. Notably, the thylakoids suffered from severe damage, showing disordered stacking and arrangement as well as a significant reduction in total quantity. After the 96-h recovery, the cellular structure partially recovered, as manifested by the relatively clear laminar

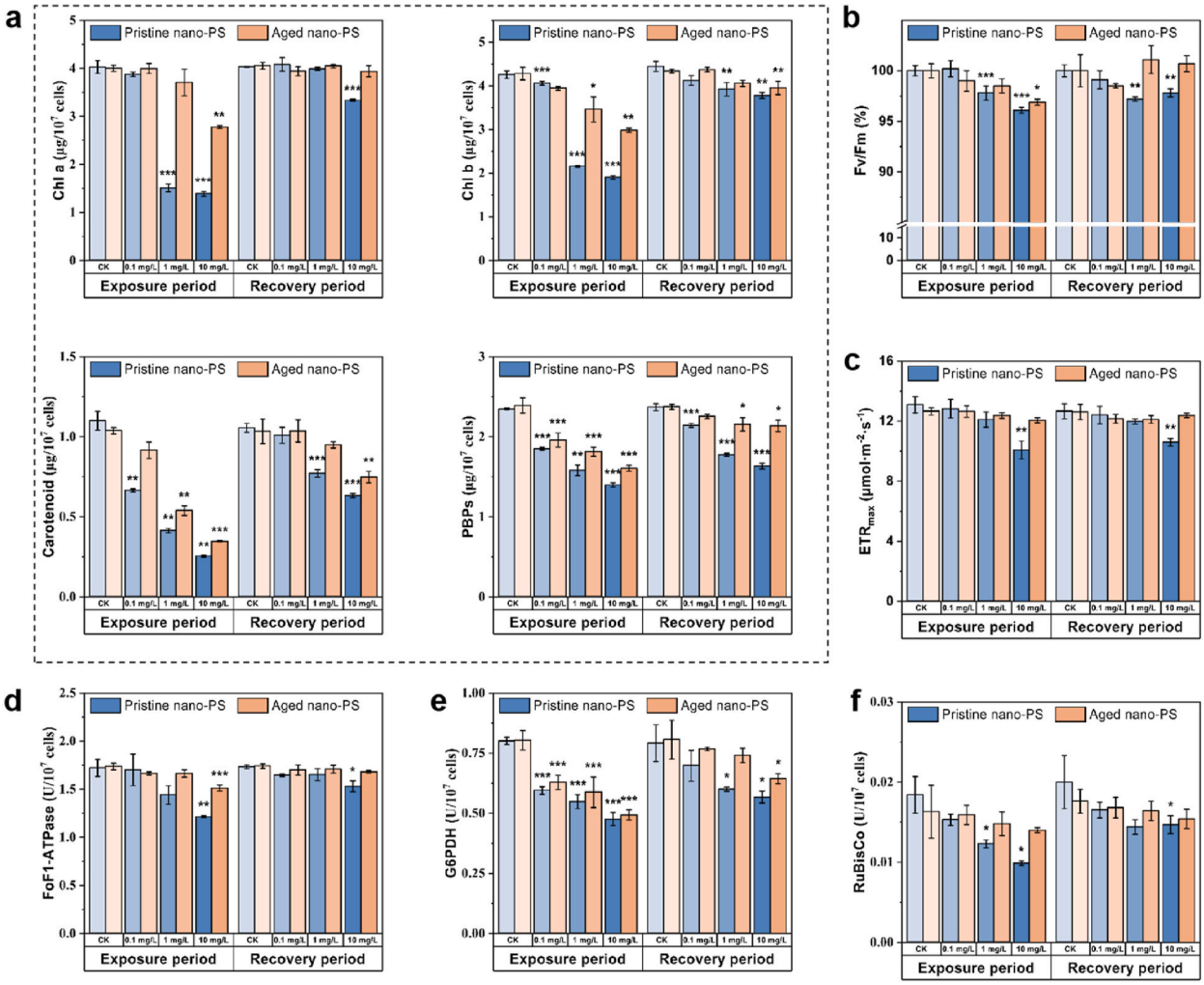

Fig. 4. Inhibition and recovery of photosynthetic process in the algae exposed to nano-PS. (a) Content of photosynthetic pigments including chlorophyll *a*, chlorophyll *b*, carotenoids, and phycobiliproteins (PBPs); Values of (b) F_v/F_m and (c) ETR_{max}; activities of three key enzyme including (d) FoF1-ATPase, (e) G6PDH, and (f) RuBisCo. Error bars represent standard deviations (n = 3). * denotes significant differences from the controls, $^*P < 0.05$, $^{**}P < 0.01$, $^{***}P < 0.001$.

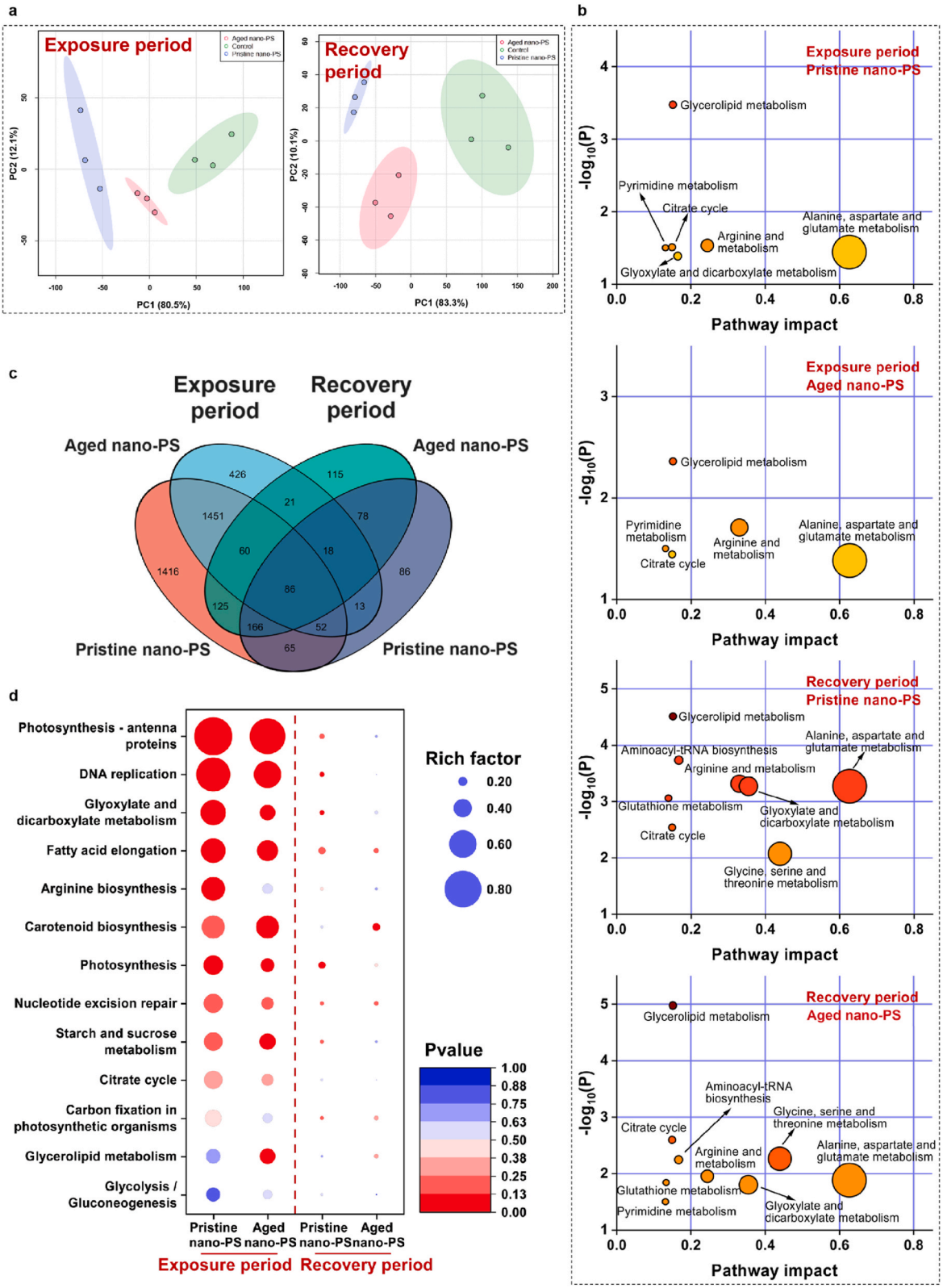

Fig. 5. Metabolic and transcription analyses of algae cells exposed to 10 mg/L nano-PS in the exposure and recovery periods. (a) PCA score plots of the metabolic profiles in the exposure and recovery periods; (b) significantly changed metabolic pathways; (c) number of DEGs in different treatment groups; (d) KEGG enrichment of DEGs between control and different treatments.

arrangement and the recovery of thylakoid quantity. Reorganization of thylakoids has been previously reported to be a mechanism in response to external environmental stressors in photosynthetic organisms [36]. Comparatively, the aged nano-PS caused less damage to the cellular structure than the pristine nano-PS, especially during the recovery period, as multiple organelles reverted to normal state except for plasmolysis. Since thylakoids serve as the major sites for light reactions, damage to the thylakoids suggested that the photosynthesis of algal cells might be adversely affected by nano-PS.

3.4. Effect of nano-PS on the photosynthetic process of algae

Photosynthetic pigments located in the chloroplasts play a vital role in capturing light and converting it into chemical energy, making chloroplasts the primary site for photosynthesis. As shown in Fig. 4a, the exposure to pristine nano-PS at higher concentrations (1 and 10 mg/L) reduced the levels of chlorophyll *a* and chlorophyll *b* by up to 62–66 % and 49–55 %, respectively, while the aged nano-PS caused 7–31 % and 19–30 % reductions of these two pigments, respectively. After a recovery period, levels of chlorophyll *a* and chlorophyll *b* in nano-PS-exposed algae sharply increased to levels comparable to or slightly lower than those of the blank controls, indicating dramatic recovery of chlorophylls from nano-PS exposure. During both exposure and recovery periods, the contents of carotenoids and phycobiliproteins declined with increasing nano-PS concentration and were higher in the algal cells exposed to the aged nano-PS at each concentration. Similarly, a reduction in chlorophylls and carotenoid levels has also been observed in the microalgae *P. helgolandica* after exposure to 70 nm PS [10]. Overall, exposure to nano-PS reduced the levels of the photosynthetic pigments in algal cells and thereby weakened the light capture ability, but the inhibitory effect was alleviated by aging.

Given the crucial role of photosynthetic pigments in light capture and conversion, decrease in photosynthetic pigments may affect the electron transport and subsequent carbon fixation. F_v/F_m value represents the maximum efficiency of PSII in converting absorbed light energy into chemical energy. The F_v/F_m values of the algae significantly decreased after the 96-h exposure to 1 and 10 mg/L pristine nano-PS, and a slight but significant recovery of F_v/F_m was observed in the 10 mg/L treatment group at the recovery stage (Fig. 4b). As compared with the pristine nano-PS treatments, the F_v/F_m values of the aged nano-PS-exposed algae were largely higher, and completely recovered after the 96-h recovery. ETR_{max} represents the maximum photosynthetic electron transport rate. In the group treated with 10 mg/L pristine nano-PS, ETR_{max} significantly decreased from 13.1 to 10.1 μmol m^{-2} s^{-1} during the exposure period, and remained nearly constant after recovery (Fig. 4c), indicating the persistence of the inhibitory effect. By comparison, there was no significant difference in ETR_{max} among the aged nano-PS treatments at any stage. The above results collectively demonstrated that nano-PS could inhibit the light reactions of algae, while the inhibitory effect of aged nano-PS was less remarkable.

FoF_1-ATPase and G6PDH are not directly involved in photosynthetic carbon fixation, but the ATP and NADPH they produce participate in the Calvin cycle as an energy source and a reducing agent, respectively. As the initiating enzyme of the Calvin cycle, the activity of RuBisCo indicates the strength of carbon dioxide fixation. During the exposure period, the activity of FoF_1-ATPase in pristine nano-PS-exposed algae decreased in a dose-dependent manner and was relatively lower compared to the aged nano-PS, particularly at 10 mg/L ($P = 0.002$) (Fig. 4d). During the recovery period, the FoF_1-ATPase activities in algal cells exposed to both nano-PS were largely restored, except for the 10 mg/L pristine nano-PS treatment group. As shown in Fig. 4e and f, the activities of G6PDH and RuBisCo decreased significantly with the increase of pristine nano-PS concentration after the 96-h exposure, with a maximum inhibition rate of 41 % and 46 % at 10 mg/L, respectively. After the recovery period, the G6PDH and RuBisCo activities of the algae exposed to pristine nano-PS increased. Similar tendency was observed in the case of aged nano-PS exposure. Nevertheless, the algae exposed to the aged nano-PS basically exhibited higher RuBisCo activity than the pristine nano-PS-exposed algae. Suppressed FoF_1-ATPase and G6PDH activities would impede the photosynthetic phosphorylation in algae, resulting in insufficient production of ATP and NADPH. Retardation of Calvin cycle along with the deficiency of ATP and NADPH would probably inhibit the carbon fixation and conversion, which was in line with the decreased CO_2 fixation rates and glucose contents in nano-PS exposed algae.

3.5. Molecular mechanisms of inhibitory effect on photosynthetic carbon fixation

A total of over 80 metabolites were identified through GC-MS analysis, with approximately 400 peaks examined for each sample during the exposure and recovery periods. PCA results showed a significant separation among the metabolites of the pristine and aged nano-PS treated algae and the control algae at both the exposure and recovery stages (Fig. 5a), suggesting that nano-PS disrupted the metabolism of algal cells and that the disruption remained obvious after recovery. Metabolic heat maps and metabolic pathway maps indicated that both materials primarily disturbed the processes associated with carbohydrate, amino acid, and lipid metabolism within algal cells (Fig. 5b–S2). During the exposure period, perturbation in glyoxylate and dicarboxylate metabolism was only observed in the pristine nano-PS treatments. Some intermediate metabolites of glyoxylate and dicarboxylate metabolism, such as citrate, aconitate, isocitrate, and oxaloacetate, are involved in the tricarboxylic acid (TCA) cycle. It indicated that the pristine nano-PS had a greater effect on the energy metabolism than the aged nano-PS. After recovery, three additional pathways, namely aminoacyl-tRNA biosynthesis, glutathione metabolism, and glycine-serine-threonine metabolism were found to be affected in algae exposed to both the pristine and the aged nano-PS; meanwhile, a remarkable decrease in glycine and serine contents were observed at this stage. This may be because substantial amounts of glycine and serine were utilized at the recovery stage to synthesize vital compounds including proteins, nucleic acids, and vitamins for resisting environmental stresses and restoring cell functions [37,38].

Compared to the blank control, there were 3421 and 2127 DEGs in the pristine and aged nano-PS exposed algae at the exposure stage, which respectively dropped to 564 and 669 at the recovery stage (Fig. 5c). This finding implied that both pristine and aged nano-PS induced changes in gene expression with the former having a greater impact. The KEGG enrichment analysis showed that 13 pathways were enriched in the nano-PS treated groups. Among the enriched pathways, the photosynthesis-antenna proteins,

photosynthesis and carbon fixation in photosynthetic organisms were directly associated with photosynthetic carbon fixation (Fig. 5d). Though the carotenoid biosynthesis is not directly involved in photosynthetic carbon fixation, carotenoids play a protective role in chlorophyll. Moreover, fatty acid, sugar, amino acid, and genetic material related pathways were enriched in the nano-PS treatment groups, which was consistent with the observed metabolic disorders. The enrichment of all the 13 pathways was much lower in the recovery stage than that in the exposure stage, demonstrating partial recovery from nano-PS toxicity. Compared to the pristine nano-PS, the exposure to the aged nano-PS resulted in less enrichment of all the enriched pathways except for carotenoid biosynthesis and glycerolipid metabolism.

Conjoint analysis of metabolome and transcriptome can provide a comprehensive understanding of mechanisms underlying the

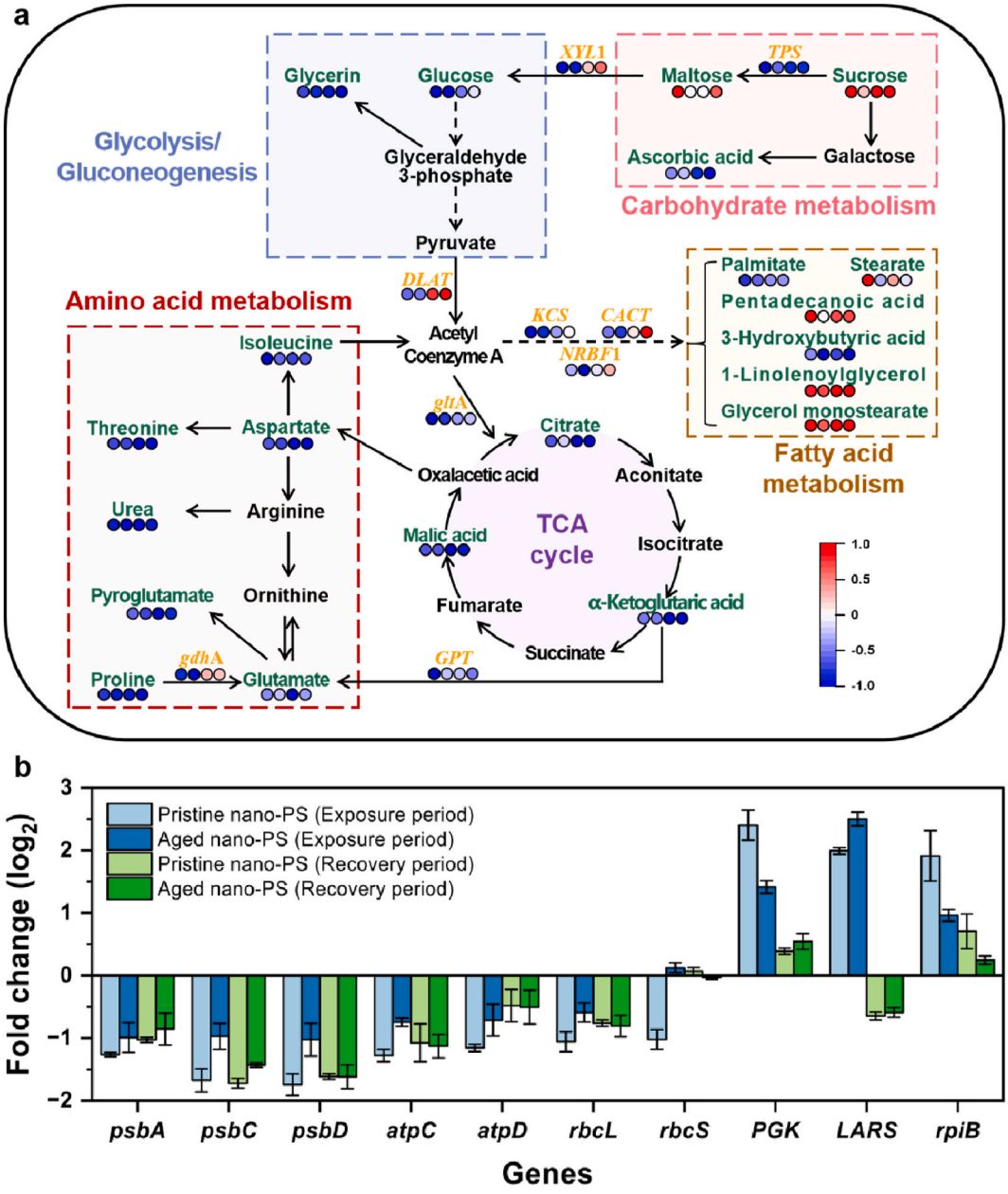

Fig. 6. Molecular mechanisms studied by metabolic and transcription analysis. (a) Pathways of significantly changed metabolites and DEGs. Green and yellow texts respectively represent differential metabolites and DEGs. The four circles below the colored texts from left to right represent the pristine nano-PS treatment during the exposure period, the aged nano-PS treatment during the exposure period, the pristine nano-PS treatment during the recovery period, and the aged nano-PS treatment during the recovery period, respectively. The colors in the circles represent the relative levels of metabolites and gene expressions to the control groups. (b) Expression levels of the genes related to chloroplasts. Error bars represent standard deviations (n = 4).

algal toxicity of nano-PS (Fig. 6a). Despite a significant accumulation of sucrose and maltose (except for maltose in the aged nano-PS exposed group), downregulation of *TPS* and *XYL*1, genes encoding the key enzymes involved in sucrose-to-maltose and maltose-to-glucose conversion, respectively, led to a decrease in glucose content in the nano-PS exposed groups in the exposure period. Compared with the pristine nano-PS, the content of maltose and glucose were relatively lower and the transcription of *TPS* was less inhibited after the 96-h exposure to the aged nano-PS. Increased maltose could protect proteins, membranes, and photosynthetic electron transport chain and was supposed to be a protective mechanism against environmental stress [39,40]. After recovery, the up-regulation of gene *XYL*1 led to the recovery of glucose level. Genes *DLAT* and *glt*A respectively encode dihydrolipoamide S-acetyltransferase and citrate synthase, which facilitate the entry of glycolytic pyruvate into the TCA cycle. Downregulation of these two genes led to the decreased levels of citrate, α-Ketoglutaric acid, and malic acid which are intermediates from the TCA cycle, suggesting suppressed TCA cycling and ultimately insufficient ATP production at the exposure stage. During the recovery period, gene *DLAT* was up-regulated, catalyzing the conversion of pyruvate to acetyl coenzyme A (acetyl-CoA) to supplement the suppressed TCA cycling. The decreased expression of gene *GPT* encoding alanine transaminase indicated that nano-PS inhibited the transformation between α-ketoglutaric acid and L-glutamate, thereby reducing the level of L-glutamate. As a precursor for chlorophyll synthesis, reduced L-glutamate might hinder chlorophyll conversion within algal cells, ultimately impairing photosynthetic capacity [41,42]. L-proline plays a vital role in regulating the intracellular ratio of NADP/NADPH and the metabolic processes in the Calvin cycle [43,44]. The decrease in L-proline content demonstrated that nano-PS had a direct negative effect on the process of carbon fixation. Alternatively, acetyl-CoA is also a critical precursor for endogenous fatty acid synthesis. Downregulation of the related genes *KCS*, *CACT*, and *NRBF*1 resulted in disrupted fatty acid metabolism after nano-PS exposure. Specifically, the increase of pentadecanoic acid, glycerol monostearate, and 1-linolenoylglycerol in all the nano-PS treatments would collectively inhibit α-glucosidase activity, thereby reducing glucose production [45,46]. The contents of stearate increased in the pristine nano-PS treatments with higher levels at the exposure stage, but slightly decreased in the aged nano-PS treatments. Elevated stearate levels would impair chloroplast function by degrading phycobiliproteins within the thylakoid membranes and impeding photosynthetic electron transport [47]. Additionally, the ornithine-urea metabolism in algae is a critical metabolic pathway for converting carbon into nitrogenous compounds [48]. The content of urea, a downstream product of amino acids, was significantly reduced in all the nano-PS treatments, suggesting a decrease in the carbon fixation capacity of the algal cells.

The expressions of photosynthesis-related genes are shown in Fig. 6b. Genes *psb*A, *psb*C, and *psb*D, which are associated with photosystem II, were down-regulated in all the nano-PS treatments, suggesting possible impairment in light-trapping ability and electron transport; this was consistent with the observed decrease in photosynthetic pigments and ETR_{max}. Moreover, the suppressed activity of FoF1-ATPase and expression of its associated genes (*atp*C and *atp*D) as well as the inhibited G6PDH activity in the nano-PS exposed algae may result in insufficient energy supply for the carbon fixation. Notably, the expression of photosystem II and ATP synthesis related genes were largely less inhibited in the aged nano-PS exposed group at the exposure stage as compared to the pristine nano-PS exposed group. The Calvin cycle might be inhibited as indicated by the reduced activity of RuBisCo and down-regulation of its related genes *rbcL* and *rbcS*. However, gene *PGK* encoding phosphoglycerate kinase (PGK) that catalyzes the conversion of glycerate-3-phosphate in the Calvin cycle was up-regulated in the nano-PS treatments. The involvement of PGK in abiotic stress tolerance has previously been observed in *Synechocystis* sp [49]. Despite the dramatic recovery of the expression of *PGK* in both nano-PS treatments after recovery, the pristine nano-PS was significantly more effective in promoting the expression of *PGK* than the aged nano-PS at the exposure stage. The exposure to nano-PS up-regulated gene *LARS* encoding leucyl-tRNA synthetase that involves in protein synthesis, which might be responsible for the changes in metabolites associated with aminoacyl-tRNA biosynthesis. At the recovery stage, the expression of gene *LARS* was almost fully recovered. Gene *rpiB* involved in the inter-conversion of ribose 5-phosphate and ribulose 5-phosphate, which is essential to the pentose phosphate pathway as well as the Calvin cycle. The increased expression of gene *rpiB* after the exposure to nano-PS, especially the pristine nano-PS, suggested the perturbation in the Calvin cycle and the pentose phosphate pathway.

4. Conclusions

The present study investigated the effect of UV-aging on the toxicity of nano-PS toward *C. vulgaris*, especially the inhibitory effect on carbon fixation. Recovery of the toxic effects after a 96-h recovery period was also studied for a comprehensive assessment of the nanoplastic toxicity. Nano-PS inhibited the growth of *C. vulgaris* with the pristine nano-PS being more toxic. Despite the partial recovery of growth, pristine nano-PS were also more effective in inhibiting the algal growth than aged nano-PS in the recovery period. Similarly, nano-PS inhibited the photosynthetic carbon fixation as characterized by reduced CO_2 fixation rate and glucose production of algal cells, while UV-aging alleviated the inhibitory effect in both exposure and recovery periods. It was found that aging improved the hydrophilicity of nano-PS, resulting in weaker agglomeration with algal cells and thus less severe cell damage. Damage to the chloroplasts especially the thylakoids induced by nano-PS inhibited the light reactions (*i.e.*, light trapping and conversion, electron transport, and photophosphorylation) by disturbing the synthesis of photosynthetic pigments, which led to insufficient ATP production for the subsequent carbon fixation process. The RuBisCo activity and the expression of its associated genes *rbc*L and *rbc*S were suppressed, indicating inhibition of the Calvin cycle. Moreover, nano-PS exposure caused disturbances in the metabolisms of carbohydrates, amino acids, and lipids, which directly or indirectly interfered with the Calvin cycle and glucose formation of the algae. Given the tremendous contribution of microalgae to the global carbon fixation and the ubiquity of nanoplastics in the aquatic systems, the potential threat of nanoplastics to the global carbon cycle should be of great concern. Furthermore, the environmental behavior of nanoplastics in aquatic systems is affected by many parameters, including types and physicochemical properties of nanoplastics, water quality parameters, UV irradiation and natural organic matters, etc. Therefore, future studies concerning the toxicity of nanoplastics

should taking different parameters into consideration. Specifically, environmentally relevant conditions, such as application of nanoplastics derived from real-life plastic products and the main environmental aging processes (eco-corona formation and photo-aging), should be considered for a more environmentally realistic toxicological assessment of nanoplastics.

Data availability statement

Data will be made available on request.

CRediT authorship contribution statement

Ziyi Sun: Writing – original draft, Methodology, Formal analysis, Data curation, Conceptualization. **Shuang Zhang:** Validation. **Tianying Zheng:** Data curation. **Caijiao He:** Data curation. **Jiang Xu:** Data curation. **Daohui Lin:** Writing – review & editing, Supervision, Funding acquisition. **Luqing Zhang:** Writing – review & editing, Supervision.

Declaration of competing interest

The authors declare no competing financial interest.

Acknowledgement

This research was supported by the National Natural Science Foundation of China (42192573, U21A20163, and 42307494).

Appendix A. Supplementary data

Supplementary data to this article can be found online at https://doi.org/10.1016/j.heliyon.2024.e29814.

References

[1] A. Isobe, S. Iwasaki, K. Uchida, T. Tokai, Abundance of non-conservative microplastics in the upper ocean from 1957 to 2066, Nat. Commun. 10 (1) (2019) 417.
[2] C. Larue, G. Sarret, H. Castillo-Michel, A.E. Pradas del Real, A critical review on the impacts of nanoplastics and microplastics on aquatic and terrestrial photosynthetic organisms, Small 17 (20) (2021).
[3] C.H. Wang, J. Zhao, B.S. Xing, Environmental source, fate, and toxicity of microplastics, J. Hazard Mater. 407 (2021) 17.
[4] X.D. Sun, X.Z. Yuan, Y. Jia, L.J. Feng, F.P. Zhu, S.S. Dong, J. Liu, X. Kong, H. Tian, J.L. Duan, Z. Ding, S.G. Wang, B. Xing, Differentially charged nanoplastics demonstrate distinct accumulation in *Arabidopsis thaliana*, Nat. Nanotechnol. 15 (9) (2020) 755–760.
[5] H. Shin, C.B. Jeong, Metabolism deficiency and oxidative stress induced by plastic particles in the rotifer Brachionus plicatilis: common and distinct phenotypic and transcriptomic responses to nano- and microplastics, Mar. Pollut. Bull. 182 (2022) 113981.
[6] B.X. Luo, J.M. Li, M. Wang, X.X. Zhang, Y. Mi, J. Xiang, S.J. Gong, Y.R. Zhou, T.W. Ma, Chronic toxicity effects of sediment-associated polystyrene nanoplastics alone and in combination with cadmium on a keystone benthic species *Bellamya aeruginosa*, J. Hazard Mater. 433 (2022) 11.
[7] Y. Wu, P. Guo, X. Zhang, Y. Zhang, S. Xie, J. Deng, Effect of microplastics exposure on the photosynthesis system of freshwater algae, J. Hazard Mater. 374 (2019) 219–227.
[8] S.H. Ho, M.C. Chan, C.C. Liu, C.Y. Chen, W.L. Lee, D.J. Lee, J.S. Chang, Enhancing lutein productivity of an indigenous microalga *Scenedesmus obliquus* FSP-3 using light-related strategies, Bioresour. Technol. 152 (2014) 275–282.
[9] S.S. Correa, J. Schultz, K.J. Lauersen, A.S. Rosado, Natural carbon fixation and advances in synthetic engineering for redesigning and creating new fixation pathways, J. Adv. Res. 47 (2023) 75–92.
[10] S. Wang, M. Liu, J. Wang, J. Huang, J. Wang, Polystyrene nanoplastics cause growth inhibition, morphological damage and physiological disturbance in the marine microalga *Platymonas helgolandica*, Mar. Pollut. Bull. 158 (2020).
[11] C. Zhang, X. Chen, J. Wang, L. Tan, Toxic effects of microplastic on marine microalgae *Skeletonema costatum*: interactions between microplastic and algae, Environ. Pollut. 220 (Pt B) (2017) 1282–1288.
[12] W.Y. Cheah, P.L. Show, J.S. Chang, T.C. Ling, J.C. Juan, Biosequestration of atmospheric CO_2 and flue gas-containing CO_2 by microalgae, Bioresour. Technol. 184 (2015) 190–201.
[13] X.Q. You, M.T. You, Y.T. Lyu, G.Y. Peng, W.L. Sun, Single and combined exposure to micro(nano)plastics and azithromycin disturbing the photosynthetic carbon fixation of *Synechocystis sp*, Environ. Sci.: Nano 9 (12) (2022) 4354–4366.
[14] M. Han, C. Zhu, S. Tang, J. Liang, D. Li, Y. Guo, Z. Zuraini, Q. Si, Q. Jiang, The effects of a polystyrene nanoplastic on the immune response and gut microbiota of *Eriocheir sinensis* and its post-recovery state, Aquat. Toxicol. 262 (2023).
[15] Y.K. Song, S.H. Hong, M. Jang, G.M. Han, S.W. Jung, W.J. Shim, Combined effects of UV exposure dration and mechanical abrasion on microplastic fragmentation by polymer type, Environ. Sci. Technol. 51 (8) (2017) 4368–4376.
[16] H. Chen, X. Hua, Y. Yang, C. Wang, L. Jin, C. Dong, Z. Chang, P. Ding, M. Xiang, H. Li, Y. Yu, Chronic exposure to UV-aged microplastics induces neurotoxicity by affecting dopamine, glutamate, and serotonin neurotransmission in *Caenorhabditis elegans*, J. Hazard Mater. 419 (2021) 126482.
[17] Y. Zhong, Q. Ding, Z. Huang, X. Xiao, X. Han, Y. Su, D. Wang, J. You, Influence of ultraviolet-aging and adsorbed pollutants on toxicological effects of polyvinyl chloride microplastics to zebrafish, Environ. Pollut. 316 (Pt 2) (2023) 120617.
[18] Z. Liu, Y. Zhu, S. Lv, Y. Shi, S. Dong, D. Yan, X. Zhu, R. Peng, A.A. Keller, Y. Huang, Quantifying the dynamics of polystyrene microplastics UV-aging process, Environ. Sci. Technol. Lett. 9 (1) (2021) 50–56.
[19] D. Wu, L. Deng, T. Wang, W. Du, Y. Yin, H. Guo, Aging process does not necessarily enhance the toxicity of polystyrene microplastics to *Microcystis aeruginosa*, Sci. Total Environ. 882 (2023) 163608.
[20] K. Sridhar, A.L. Charles, In vitro antioxidant activity of *Kyoho* grape extracts in DPPH and ABTS assays: estimation methods for EC_{50} using advanced statistical programs, Food Chem. 275 (2019) 41–49.
[21] S. Ma, K.J. Zhou, K. Yang, D.H. Lin, Heteroagglomeration of oxide nanoparticles with algal cells: effects of particle type, ionic strength and pH, Environ. Sci. Technol. 49 (2) (2015) 932–939.

[22] S.Y. Chiu, C.Y. Kao, C.H. Chen, T.C. Kuan, S.C. Ong, C.S. Lin, Reduction of CO_2 by a high-density culture of *Chlorella sp.* in a semicontinuous photobioreactor, Bioresour. Technol. 99 (9) (2008) 3389–3396.
[23] Y.A. Lim, M.N. Chong, S.C. Foo, I.M.S.K. Ilankoon, Analysis of direct and indirect quantification methods of CO_2 fixation via microalgae cultivation in photobioreactors: a critical review, Renew. Sustain. Energy Rev. 137 (2021).
[24] E.M. Johnson, K. Kumar, D. Das, Physicochemical parameters optimization, and purification of phycobiliproteins from the isolated *Nostoc sp*, Bioresour. Technol. 166 (2014) 541–547.
[25] H.K. Lichtenthaler, A.R. Wellburn, Determinations of total carotenoids and chlorophylls a and b of leaf extracts in different solvents, Biochem. Soc. Trans. 11 (5) (1983) 591–592.
[26] E. Smith, The influence of light and carbon dioxide on photosynthesis, J. Gen. Physiol. 20 (6) (1937) 807–830.
[27] Y. Liu, T. Wu, J.C. White, D. Lin, A new strategy using nanoscale zero-valent iron to simultaneously promote remediation and safe crop production in contaminated, soil Nat Nanotechnol 16 (2) (2021) 197–205.
[28] L.Q. Zhang, C. Lei, K. Yang, J.C. White, D.H. Lin, Cellular response of *Chlorella pyrenoidosa* to oxidized multi-walled carbon nanotubes, Environ. Sci.: Nano 5 (10) (2018) 2415–2425.
[29] G. Liu, Z. Zhu, Y. Yang, Y. Sun, F. Yu, J. Ma, Sorption behavior and mechanism of hydrophilic organic chemicals to virgin and aged microplastics in freshwater and seawater, Environ. Pollut. 246 (2019) 26–33.
[30] J. Wen, H. Sun, Z.X. Liu, X.Y. Zhu, Z.M. Qin, E.R. Song, Y. Song, Aging processes dramatically alter the protein corona constitution, cellular internalization, and cytotoxicity of polystyrene nanoplastics, Environ. Sci. Technol. Lett. 9 (11) (2022) 962–968.
[31] S. Roy, C.Y. Yue, Y.C. Lam, Z.Y. Wang, H. Hu, Surface analysis, hydrophilic enhancement, ageing behavior and flow in plasma modified cyclic olefin copolymer (COC)-based microfluidic devices, Sensor Actuat B-Chem 150 (2) (2010) 537–549.
[32] Y. Wang, D.J. Stessman, M.H. Spalding, The CO_2 concentrating mechanism and photosynthetic carbon assimilation in limiting CO_2: how *Chlamydomonas* works against the gradient, Plant J. 82 (3) (2015) 429–448.
[33] M.-A. Shahbazi, M. Hamidi, E.M. Mäkilä, H. Zhang, P.V. Almeida, M. Kaasalainen, J.J. Salonen, J.T. Hirvonen, H.A. Santos, The mechanisms of surface chemistry effects of mesoporous silicon nanoparticles on immunotoxicity and biocompatibility, Biomaterials 34 (31) (2013) 7776–7789.
[34] A. Bellingeri, S. Casabianca, S. Capellacci, C. Faleri, E. Paccagnini, P. Lupetti, A.A. Koelmans, A. Penna, I. Corsi, Impact of polystyrene nanoparticles on marine diatom *Skeletonema marinoi* chain assemblages and consequences on their ecological role in marine ecosystems, Environ. Pollut. 262 (2020) 114268.
[35] V. Nava, B. Leoni, A critical review of interactions between microplastics, microalgae and aquatic ecosystem function, Water Res. 188 (2021) 116476.
[36] B. Demmig-Adams, O. Muller, J.J. Stewart, C.M. Cohu, W.W. Adams, Chloroplast thylakoid structure in evergreen leaves employing strong thermal energy dissipation, J. Photochem. Photobiol., B 152 (Pt B) (2015) 357–366, 3rd.
[37] X. Fu, B.J. Walker, Dynamic response of photorespiration in fluctuating light environments, J. Exp. Bot. 74 (2) (2023) 600–611.
[38] Z.S. Zhang, M.J. Liu, R. Scheibe, J. Selinski, L.T. Zhang, C. Yang, X.L. Meng, H.Y. Gao, Contribution of the alternative respiratory pathway to PSII photoprotection in C3 and C4 pants, Mol. Plant 10 (1) (2017) 131–142.
[39] Y. Lu, T.D. Sharkey, The importance of maltose in transitory starch breakdown, Plant Cell Environ. 29 (3) (2006) 353–366.
[40] S.E. Weise, A.P. Weber, T.D. Sharkey, Maltose is the major form of carbon exported from the chloroplast at night, Planta 218 (3) (2004) 474–482.
[41] H. Ito, S. Takaichi, H. Tsuji, A. Tanaka, Properties of synthesis of chlorophyll a from chlorophyll b in cucumber etioplasts, J. Biol. Chem. 269 (35) (1994) 22034–22038.
[42] J. Zhang, D. Yang, M. Li, L. Shi, Metabolic profiles reveal changes in wild and cultivated soybean seedling leaves under salt stress, PLoS One 11 (7) (2016) e0159622.
[43] M. Li, R. Guo, Y. Jiao, X. Jin, H. Zhang, L. Shi, Comparison of salt tolerance in soja based on metabolomics of seedling roots, Front. Plant Sci. 8 (2017) 1101.
[44] I. Mariam, M.S. Kareya, A.A. Nesamma, P.P. Jutur, Delineating metabolomic changes in native isolate *Aurantiochytrium* for production of docosahexaenoic acid in presence of varying carbon substrates, Algal Res. 55 (2021).
[45] N. Li, Q. Li, X. He, X. Gao, L. Wu, M. Xiao, W. Cai, B. Liu, F. Zeng, Antioxidant and anti-aging activities of *Laminaria japonica* polysaccharide in *Caenorhabditis elegans* based on metabonomic analysis, Int. J. Biol. Macromol. 221 (2022) 346–354.
[46] S. Murugesu, Z. Ibrahim, Q.U. Ahmed, B.F. Uzir, N.I. Nik Yusoff, V. Perumal, F. Abas, K. Shaari, A. Khatib, Identification of alpha-glucosidase inhibitors from *Clinacanthus nutans* leaf extract using liquid chromatography-mass spectrometry-based metabolomics and protein-ligand interaction with molecular docking, J Pharm Anal 9 (2) (2019) 91–99.
[47] S. Ouyang, X. Hu, Q. Zhou, X. Li, X. Miao, R. Zhou, Nanocolloids in natural water: isolation, characterization, and toxicity, Environ. Sci. Technol. 52 (8) (2018) 4850–4860.
[48] A.E. Allen, C.L. Dupont, M. Obornik, A. Horak, A. Nunes-Nesi, J.P. McCrow, H. Zheng, D.A. Johnson, H. Hu, A.R. Fernie, C. Bowler, Evolution and metabolic significance of the urea cycle in photosynthetic diatoms, Nature 473 (7346) (2011) 203–207.
[49] Y. Tsukamoto, Y. Fukushima, S. Hara, T. Hisabori, Redox control of the activity of phosphoglycerate kinase in *Synechocystis sp* PCC6803, Plant Cell Physiol. 54 (4) (2013) 484–491.